Scanning Electrochemical Microscopy. 43. Investigation of Oxalate Oxidation and Electrogenerated Chemiluminescence across the Liquid−Liquid Interface†

Frédéric Kanoufi,‡,§ Céline Cannes,‡ Yanbing Zu,‡ and Allen J. Bard*,‡

Department of Chemistry and Biochemistry, The University of Texas at Austin, Austin, Texas 78712, and Laboratoire Environnement et Chimie Analytique, ESPCI, 10 rue Vauquelin, 75231 Paris Cedex 05, France

Received: March 7, 2001; In Final Form: June 15, 2001

To treat the problem of oxalate oxidation in an aqueous phase by a Ru(III) species (mediator) generated in an immiscible nonaqueous phase (benzonitrile) at a scanning electrochemical microscope (SECM tip), the theory of the feedback mode of the SECM is extended to include both finite heterogeneous electron transfer (ET) kinetics at the substrate and homogeneous decomposition of the mediator. As for the classical electrochemical (EC) scheme, a zone diagram is constructed showing pure ET heterogeneous kinetic control, pure homogeneous kinetic (C) control (insulating behavior), and mixed EC kinetic control. The model allows interpretation of the anomalous approach curves obtained for oxalate oxidation by a ruthenium(III) coordination complex at the benzonitrile (BN)−water interface and allows calculation of the rate constant for the ET at the liquid−liquid interface. Attempts are made to relate these rates to the homogeneous rate constant in terms of Marcus theory. The second ET (oxidation of $CO_2^{\bullet-}$) at the liquid−liquid interface generates an emitting excited state of the ruthenium species. The electrogenerated chemiluminescence process is related to the current crossing the interface.

Introduction

Electron transfer (ET) reactions at the liquid−liquid interface have been extensively investigated over the past 20 years[1] owing, in part, to interest in the liquid−liquid interface as an intermediate case between homogeneous and heterogeneous sites for ET.[2] Several different models have been developed to depict the ET at the interface between two immiscible electrolyte solutions (ITIES).[3−6]

Among the various techniques used to probe ET at an ITIES (e.g., cyclic voltammetry[1] or voltfluorometry[7−9] in a four-electrode cell, voltammetry in a thin-layer cell[10]), the scanning electrochemical microscope (SECM) in its feedback mode has been shown to be particularly useful in the characterization of ET kinetics.[11−19] The SECM technique has the advantage of easy separation of the contribution of electron transfer and ion transfer processes and does not require a four-electrode arrangement with an externally applied potential across the interface. Typically in these experiments, a stable redox active species, for example an oxidant, is generated at an ultramicroelectrode (UME) tip located in one liquid phase and the tip is approached to the second liquid that contains another redox species, a reductant, that can transfer an electron to the tip-generated oxidant. The tip feedback current depends on the rate of this electron transfer. In most studies this oxidant is part of a stable redox couple, thus simplifying the treatment of the kinetics and mechanism of the system. However, the SECM technique can also be used to investigate the kinetics of irreversible ET at an ITIES, such as the reduction of dibromocyclohexane by vitamin B_{12}.[20] Such studies of electrochemical catalysis are of interest in characterizing syntheses in microemulsions. Moreover, in principle, they should provide interesting information by comparing the ET rates to their homogeneous analogues in terms of ET theory.

SCHEME 1

$$Ru^{2+}_o - e \rightarrow Ru^{3+}_o \qquad \text{(tip)}$$

$$Ru^{3+}_o + C_2O_4^{2-}_w \underset{\leftarrow}{\overset{k_{ox}}{\rightarrow}} Ru^{2+}_o + C_2O_4^{\bullet-}_w \qquad \text{(ITIES)} \quad (1)$$

$$C_2O_4^{2-}_w \xrightarrow{k_2} CO_2^{\bullet-}_w + CO_2 \qquad \text{(water)} \quad (2)$$

$$Ru^{3+}_o + CO_2^{\bullet-}_w \underset{\leftarrow}{\overset{k_3}{\rightarrow}} Ru^{2+}_o + CO_2 \qquad \text{(ITIES)} \quad (3)$$

$$Ru^{3+}_o + CO_2^{\bullet-}_w \underset{\leftarrow}{\overset{k_{3^*}}{\rightarrow}} Ru^{2+\bullet}_o + CO_2 \qquad \text{(ITIES)} \quad (3^*)$$

Previous reports from this laboratory have shown that oxidation of a luminophor such as $RuL_2L'^{2+}$ in the presence of a coreactant, such as the oxalate dianion, leads to the formation of an excited state [electrogenerated chemiluminescence (ECL)], by homogeneous reaction in the aqueous phase,[21,22] either at a polymer-modified electrode,[23] or at an ITIES.[24] This latter study qualitatively demonstrated ECL at the ITIES and proposed that its occurrence was evidence of Marcus inverted region behavior. This paper is a more detailed and quantitative study of this type of ET and ECL reaction.

Based on the observation of ECL at the BN−water interface and on the homogeneous[22] or electrochemical[25] oxidation of oxalate, a mechanism of the ECE type, depicted in Scheme 1 and schematically presented in Figure 1 in the SECM configuration, can be invoked for the SECM monitored oxalate

† Part of the special issue "Royce W. Murray Festschrift".
‡ The University of Texas at Austin.
§ ESPCI.

10.1021/jp0108667 CCC: $20.00
Published on Web 08/10/2001

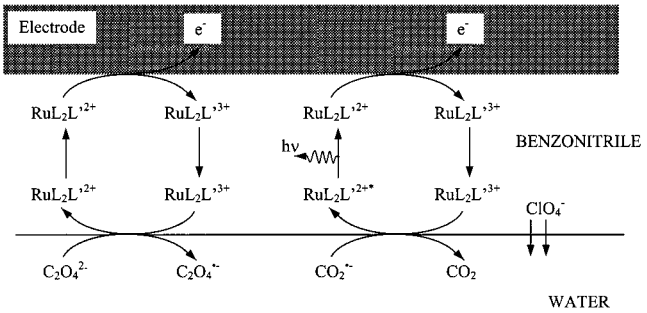

Figure 1. Schematic illustration of the reaction scheme and occurrence of ECL at the BN−water interface during oxalate oxidation by a ruthenium complex.

oxidation by $RuL_2L'^{3+}$ at the BN−water interface. In Scheme 1, Ru^{2+} represents the $RuL_2L'^{2+}$ species, and the subscripts "o" and "w" represent the organic and water phases, respectively.

The occurrence of different paths for the oxidation of the highly reducing carbon dioxide radical anion, $CO_2^{\bullet -}$, has been investigated by pulse radiolysis.[26] Oxidation by Ru^{2+} was shown to be negligible, compared to oxidation by Ru^{3+}; the latter process leads to Ru^{2+} in its excited (3*) and ground (3) states. This was interpreted not as a contradiction of the existence of the Marcus inverted region, but rather for its difficult accessibility[22] due to the high reorganization energy needed for $CO_2^{\bullet -}$ oxidation.[26,27]

In carrying out these studies, a comparison of the homogeneous and the ITIES oxalate oxidations should be straightforward. However, the SECM curves observed when approaching the tip to the ITIES presented an atypical decrease in the normalized current before a current enhancement due to mediator regeneration at the ITIES by ET to the oxalate. This unusual dip preceding the increase in current has been attributed to possible irreversible reaction between the oxidized mediator $Ru(bpy)_2C_{12}\text{-}bpy^{3+}$ (**1**) with water in the organic phase that does not regenerate $Ru(bpy)_2C_{12}\text{-}bpy^{2+}$:

$$Ru^{3+}{}_o + H_2O_o \xrightarrow{k_c} \text{product (BN)} \qquad (4)$$

Thus, such approach curve shapes, sometimes seen with a liquid/solid interface, reflect the intervention of a competitive path in addition to the simple interfacial ET. Typically this situation has been observed and treated theoretically during investigations of the generation−collection mode of electron transfer followed by a chemical reaction[28,29] or during ET at an ITIES limited by an ionic substrate transfer[11] or by substrate diffusion.[16]

The situation observed during ECL at an ITIES, which corresponds to finite heterogeneous ET (1) followed by irreversible chemical reaction of the mediator (4), has not been treated theoretically. The first part of this paper discusses the theoretical model of this situation.

The predictions of the model are then examined in the case of oxalate oxidation with different $RuL_2L'^{3+}$ complexes, presented in Table 1, at the BN−water interface. The aim of this part is to test the different models for ET at the liquid−liquid interface and to correlate the results to the homogeneous data. We then analyze the ECL in light of the electrochemical step as was done previously.[22]

Theoretical Model

Formulation of the Problem. A previous treatment of this problem (Figure 2; heterogeneous electron transfer, k_{het}, coupled to a homogeneous irreversible chemical decomposition, k_c, of the mediator) has been carried out only under the special condition where the electron transfer is diffusion controlled ($k_{het} \rightarrow \infty$). While this condition is usually easy to establish at a metal electrode, it does not fit the situation at the ITIES. We thus develop here a more general theoretical model. The principle of the measurement is presented schematically in Figure 2. For this mechanism the appropriate time-dependent diffusion equation, in cylindrical coordinates for species R and O, are

TABLE 1: Polypyridine Ruthenium Complexes

RuL_2L'	L	L′
1	bpy[a]	4,4′-$(C_{12}H_{25}O_2C)_2$bpy = C_{12}-bpy
2	bpy	5-Cl(phen)[b]
3	bpy	bpy
4	bpy	4,4′-$(CH_3)_2$bpy = dmbp
5	4,7-$(C_6H_5)_2$phen	4,7-$(C_6H_5)_2$phen
6	4,4′-$(C_6H_5)_2$phen	4,4′-$(C_6H_5)_2$phen
7	4,4′-$(CH_3)_2$bpy	4,4′-$(CH_3)_2$bpy

[a] bpy = 2,2 -bipyridine. [b] phen = 1,10-phenanthroline.

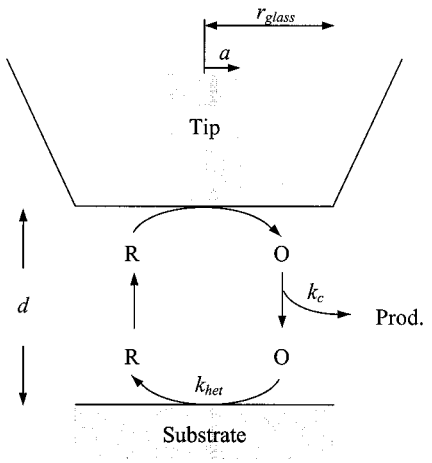

Figure 2. Schematic illustration of the general reaction of SECM feedback with finite heterogeneous electron-transfer kinetics, k_{het}, in the presence of an irreversible homogeneous reaction of O, k_c.

$$\frac{\partial c_R}{\partial t} = D\left[\frac{\partial^2 c_R}{\partial r^2} + \frac{1}{r}\frac{\partial c_R}{\partial r} + \frac{\partial^2 c_R}{\partial z^2}\right] \qquad (5)$$

$$\frac{\partial c_O}{\partial t} = D\left[\frac{\partial^2 c_O}{\partial r^2} + \frac{1}{r}\frac{\partial c_O}{\partial r} + \frac{\partial^2 c_O}{\partial z^2}\right] - k_c c_O \qquad (6)$$

where D is the diffusion coefficient, taken, for simplicity, to be the same for both species R and O, at concentrations c_R and c_O; t, r, and z represent, respectively, the time and the coordinates in the radial and normal directions to the electrode surface. The initial and boundary conditions pertinent to the problem are the following:

$$t = 0: c_R = c_R{}^*, c_O = 0 \qquad (7)$$

$$z = 0,\ 0 \le r \le a \text{ (tip)}: c_R = 0, D\frac{\partial c_R}{\partial z} = -D\frac{\partial c_O}{\partial z} \qquad (8)$$

$$z = 0,\ a \le r \le r_{glass} \text{ (glass)}: D\frac{\partial c_R}{\partial z} = D\frac{\partial c_O}{\partial z} = 0 \qquad (9)$$

$$0 < z < d,\ r = 0 \text{ (symmetry axis)}: D\frac{\partial c_R}{\partial r} = D\frac{\partial c_O}{\partial r} = 0 \qquad (10)$$

$$0 < z < d,\ r \geq r_{glass}: c_R = c_R^*, c_O = 0 \quad (11)$$

$z = d,\ 0 \leq r \leq r_{glass}$ (interface):

$$D\frac{\partial c_R}{\partial z} = -D\frac{\partial c_O}{\partial z} = k_{12}c_{R2}c_O = k_{het}c_O \quad (12)$$

where a is the tip radius; r_{glass} is the radius of the surrounding insulating glass; d is the distance between the tip and the interface; c_R^* is the value of the bulk concentration of R; k_c is the rate constant for the homogeneous decomposition of O (in s^{-1}); k_{12} is the corresponding heterogeneous bimolecular rate constant, if the model is applied to the liquid−liquid interface (the units of k_{12} are cm s^{-1} M^{-1}). The bulk concentration of the oxalate in the aqueous phase, c_{R2}^*, is assumed to be large compared to c_R^*, so it does not change appreciably during the ET reaction. When c_R^* and c_{R2}^* are comparable, consideration of diffusion of R2 in the lower phase may be required. The effect of such diffusional phenomena when no interfering homogeneous irreversible reaction in the gap occurs has been discussed elsewhere.[16] It was not taken into account here, because in our experiments the concentration of R2 was always 10 times higher than that of R.

To obtain a general solution, the following dimensionless terms were used:

$$\tau = \frac{tD}{a^2} \quad (13)$$

$$R = \frac{r}{a} \quad (14)$$

$$Z = \frac{z}{a} \quad (15)$$

$$C_i = \frac{c_i}{c_R^*} \quad (16)$$

$$K_c = \frac{k_c a^2}{D} \quad (17)$$

$$K_{het} = \frac{k_{het}a}{D} = \frac{k_{12}c_{R2}^* a}{D} \quad (18)$$

The aim of the calculation is to obtain the tip current as a function of time and the tip/interface separation, d, for different K_{het} and K_c values. The former quantity is given in its dimensionless form by

$$I_T = \frac{i_T}{i_{T,inf}} = \frac{\pi}{2}\int_0^1 \left.\frac{\partial C_R}{\partial Z}\right|_{Z=0} R\,dR \quad (19)$$

where $i_{T,inf}$ corresponds to the steady-state diffusion-limited current at a simple microdisk electrode:

$$i_{T,inf} = 4nFDc_R^* a \quad (20)$$

To solve eqs 5 and 6 numerically, we used the alternating-direction implicit (ADI) finite-difference method,[30] since this approach was shown to provide an efficient solution to a variety of SECM problems.[16,29,31,32] The method has been described elsewhere and is derived from its original detailed description for the measurement of homogeneous chemical reaction with the SECM.[28] Typically, the same finite-difference grid (exponential in both R and Z directions) was used. The ADI method involves the use of two finite-difference equations that are constructed successively, for the R and then the Z direction, at two half-time steps of $\Delta T/2$. The algorithm is based on solving two sets of tridiagonal matrix equations given by eqs A10 and A11 in ref 28 by the Thomas algorithm.[33]

For our problem, the expressions given by Table 1 in ref 28 are identical except that the following expressions replace that one defined in eq A10 of ref 28:

for R:

$$d_{j,NZ-1}(0 \leq j \leq NE+NG-2) = \lambda_Z CR_{j,NZ1-2} - (\lambda_Z - 1)^* CR_{j,NZ1-1} + \lambda_Z CO_{j,NZ1-1}/(1 + 1/(K_{het}*\Delta Z)) \quad (21)$$

for O:

$$d_{j,NZ-1}(0 \leq j \leq NE+NG-2) = \lambda_Z CO_{j,NZ1-2} - (2\lambda_Z - 1 - \lambda_Z/(1+K_{het}*\Delta Z))^* CO_{j,NZ1-1} \quad (22)$$

where the parameters can be easily understood by referring to ref 28.

In the same way, the appropriate terms to eq A11 of ref 28 are the following:

for R:

$$b^{**}_{NZ-1}(0 \leq j \leq NE+NG-1) = 1 + \lambda_Z \quad (23)$$

$$d^*_{NZ1-1}(j=0) = \{1-2\lambda_\rho(0)\}CR^*_{0,NZ-1} + 2\lambda_\rho(0)\}CR^*_{0,NZ-1} + \lambda_Z CO^{**}_{0,NZ-1}/(1 + 1/(K_{het}\Delta Z)) \quad (24)$$

$$d^*_{NZ1-1}(1 \leq j \leq NE+NG-1) = \lambda_\rho(j)\left\{1 - \frac{\Delta\rho}{2}\left[m + \frac{\exp(-ml\Delta\rho)}{s + m - m\exp(-ml\Delta\rho)}\right]\right\}CR^*_{j-1,NZ-1} + [1 - 2\lambda_\rho(j) - qK_c\Delta T/2]CR^{**}_{j,NZ-1} + \lambda_\rho(j)\left\{1 + \frac{\Delta\rho}{2}\left[m + \frac{\exp(-ml\Delta\rho)}{s + m - m\exp(-ml\Delta\rho)}\right]\right\}CR^*_{j+1,NZ-1} + \lambda_Z CO^{**}_{j,NZ-1}/(1 + 1/(K_{het}\Delta Z)) \quad (25)$$

for O:

$$b^{**}_{NZ-1}(0 \leq j \leq NE+NG-1) = 1 + 2\lambda_Z - \lambda_Z/(1 + K_{het}\Delta Z)) \quad (26)$$

Note that in eqs A8 and A9 of ref 28, in the first term in every bracketed expression, an m (which can take values of ± 1) has inadvertently been replaced by a 1; this error has been corrected in eq 25 above.

Once these corrections were made, the calculation proceeded as explained in ref 28 with 100 points in each radial zone (electrode and glass sheath) and 100 points in the z direction for $\log(d/a) = -1.2$ with an increase of 10 points per 0.1 unit increase of $\log(d/a)$.

The formulation of the problem was coded in C (Code Warrior package, Austin, TX) in double precision, and the program was executed on a Pentium III Processor personal computer.

Theoretical Results and Discussion

The model developed in this work involves two dimensionless parameters, K_c and K_{het}, that characterize respectively the homogeneous and heterogeneous fate of O generated at a tip.

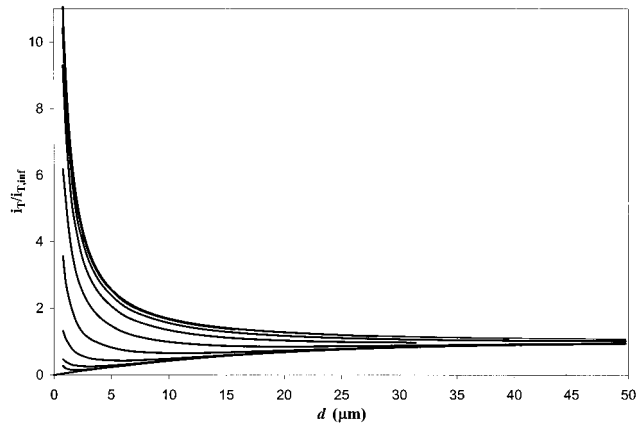

Figure 3. Variation of the simulated normalized tip current with the distance for $K_{het} = 100$ and, from top to bottom, $K_c = 0$, 0.01, 0.032, 0.1, 0.32, 1, 3.2, 10, 32, 100, ∞.

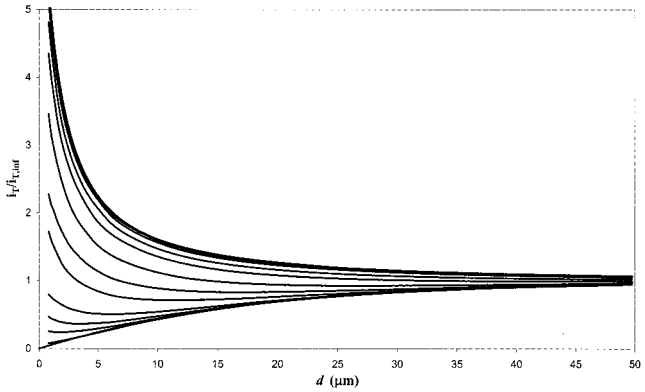

Figure 4. Variation of the simulated normalized tip current with the distance for $K_{het} = 10$ and, from top to bottom, $K_c = 0$, 0.01, 0.1, 0.2, 0.5, 1, 2, 5, 10, 20, 100, ∞.

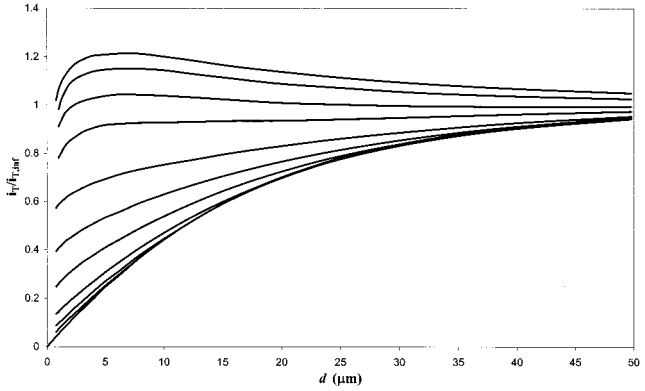

Figure 5. Variation of the simulated normalized tip current with the distance for $K_{het} = 1$ and, from top to bottom, $K_c = 0$, 0.032, 0.1, 0.2, 0.5, 1, 2, 5, 10, 20, ∞.

We devote this section to an analysis of the effect of these parameters over the normalized distance, $L = d/a$, on the steady-state tip current. This steady-state current can be obtained from the long-time behavior of the numerical calculation.

The effect of the normalized homogeneous chemical reaction K_c on the normalized approach curves is shown in Figures 3, 4, 5, and 6 for different heterogeneous rate constants, K_{het}. In each case, for values of K_c smaller than 0.01, the homogeneous chemical fate of O can be neglected; the kinetics are governed by the heterogeneous reaction. As could be intuitively expected, the deviation of the current from that predicted when there is no homogeneous reaction increases with increasing K_c.

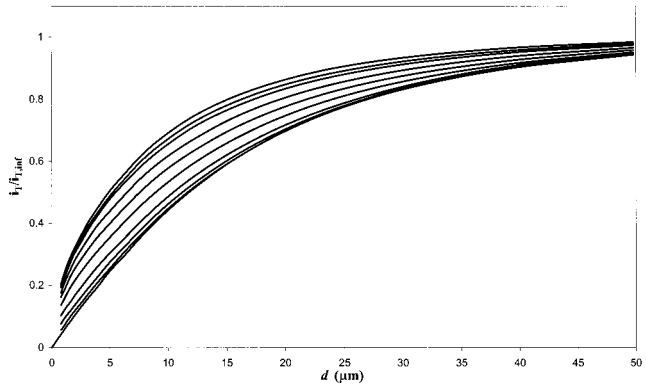

Figure 6. Variation of the simulated normalized tip current with the distance for $K_{het} = 0.1$ and, from top to bottom, $K_c = 0$, 0.01, 0.02, 0.05, 0.1, 0.2. 0.5,1, 2, ∞.

For subsequent increases in K_c, the normalized approach curve tends toward the limiting curve that corresponds to the insulator response. No feedback is observed since O is too unstable to reach the interface where it is reduced back. The situation is then kinetically limited by the homogeneous reaction. Typically, for higher values of K_{het} this situation is observed for higher values of K_c. Between these two limiting situations, the system is under a mixed kinetic control by both K_{het} and K_c.

The conditions under which these two limiting situations are observed can be more easily understood by plotting the calculated normalized current ratio as a function of log K_c. Figure 7 presents such a plot for $\log(d/a) = -1$, -0.8, -0.5 and K_{het} values ranging from 0.1 to 100. The borderline between the mixed and the heterogeneous control could be defined as the value of the normalized current at 90% of the ideal heterogeneous case (no effect of the homogeneous step). Conversely, to a reasonable approximation, the system is under pure control by the homogeneous chemical reaction, K_c, when the tip current is essentially of the insulating type, i.e., $i_T < 1.1 i_{T,ins}$. These borderlines are extrapolated from the best fit of the simulated points and are indicated in Figure 7 by dashed lines crossing the calculated working curves. The dependence of these boundaries and the zones they define on normalized distance is presented in Figure 8. This log K_{het}/log K_c zone diagram illustrates the competition between both reactions: increasing K_{het} attenuates the effect of K_c, and the mixed control zone is shifted toward higher K_c. Moreover, as already observed when the heterogeneous ET is diffusion limited,[28] the distinction between insulating behavior and mixed kinetic control is shifted to lower K_c values for greater distances; the effect of K_c is emphasized with increasing distance, d.

The extraction of the different rate constants from experimental approach curves is, in principle, more complicated, since it is a function of three independent variables (K_{het}, K_c, and L). However, some approach curves present a shallow minimum. As discussed elsewhere,[29] this minimum results from the competition between the chemical decay of O before it reaches the interface and the supply of R with increasing the gap dimension. With increasing distance, a smaller fraction of O reaches the interface, resulting in a current lower than that observed when the chemical reaction is negligible. With a larger distance, the larger supply of R diffusing in the gap tends to increase the current. A minimum, whose location and magnitude depend on the value of K_c, is observed. Note that the presence of such a minimum facilitates the data analysis, since it does not require an exact knowledge of the tip−interface distance.

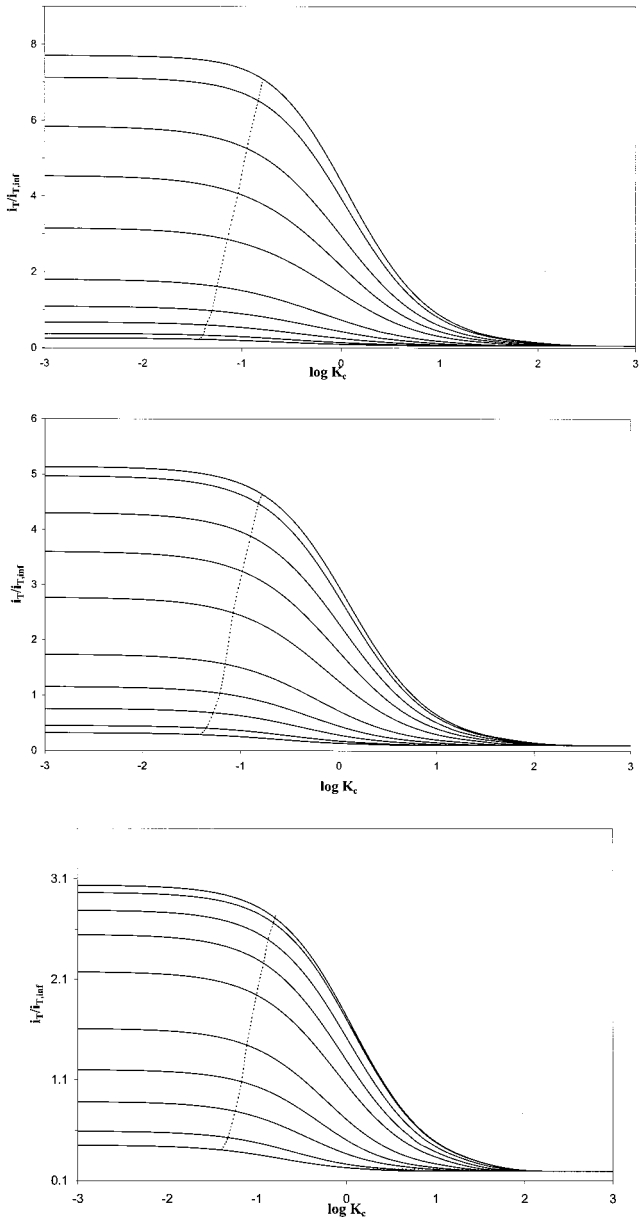

Figure 7. Variation of the simulated normalized tip current with K_c for, from bottom to top, K_{het} = 0.1, 0.2, 0.5, 1, 2, 5, 10, 20, 50, 100, and for log(d/a) = (a) −1, (b) −0.8, and (c) −0.5.

The model presented here demonstrates that one can be less restrictive in the choice of a redox mediator in the SECM investigation of heterogeneous ET. As can be seen in Figure 8, less stable redox species can be used as ET mediator for studies under steady-state feedback SECM measurements. The redox couple usefulness depends on the ET kinetics, but for k_{het} higher than 0.001 cm/s any redox species having a lifetime longer than 0.1 s can be used for ET kinetics determination. In such cases, one can distinguish the SECM feedback response from insulating behavior for gap dimensions smaller than 0.4a, i.e., 5 μm for a 25 μm diameter microdisk. For higher heterogeneous ET rate constants, redox species with lifetimes as short as 5 ms can be used with a useful response for $d \leq 0.3a$ course. On the other hand, any redox species with a lifetime of the order of a few seconds would be considered as a stable redox mediator for SECM investigation, for which the usual treatment developed for finite heterogeneous kinetics[11,13,14,20,31,35] can be used.

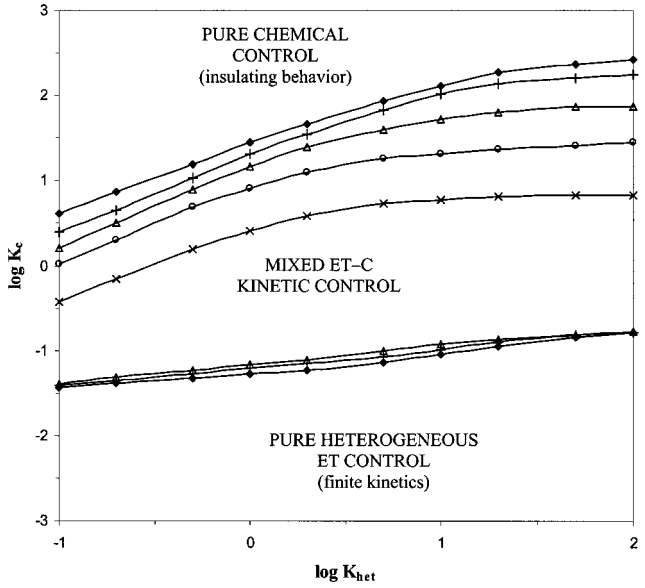

Figure 8. Diagram representing the kinetic control zones corresponding to competition between the heterogeneous reduction of O, K_{het}, and its homogeneous chemical decomposition, K_c, for different values of d/a = (◆) −1, (+) −0.8, (△) −0.5, (○) −0.2, (×) 0.

Experimental Section

Chemicals. $Na_2C_2O_4$ from J. T. Baker (Phillipsburg, NJ), $NaClO_4$, and benzonitrile from Aldrich (Milwaukee, WI) were used as received. Tetrahexylammonium perchlorate ($THAClO_4$ from Fluka Chemika) was recrystallized twice from an ethyl acetate:ether mixture (9:1) and dried under vacuum overnight at room temperature. $Ru(bpy)_3(ClO_4)_2$ was prepared by precipitation of the chloride salt (Strem Chemicals, Newburyport, MA) in a 1 M $NaClO_4$ aqueous solution and then recrystallized twice from ethanol−water (1:2). Bis(2,2′-bipyridine)ruthenium(II) chloride (Aldrich, Milwaukee, WI) was used to synthesize (Table 1) **1**,[36a] **2**, and **4**.[35b] The other $RuL_3(ClO_4)_2$ salts were synthesized according to reported procedures.[35c] The aqueous solutions were prepared from deionized water (MilliQ, Millipore).

Electrodes and Electrochemical Cells. Pt wires (25 μm diameter, Goodfellow, Cambridge, UK) were heat-sealed under vacuum in glass capillaries and then beveled to produce SECM tips as described previously.[37] The tip electrode was rinsed with ethanol and water, polished, and dried, and then rinsed with BN before each experiment. A three-electrode configuration was used in all experiments with a 0.2 mm diameter Pt wire as the counter electrode and a 0.5 mm Ag wire as a quasireference electrode. All electrodes were placed in the top organic phase. A 2 mL glass vial mounted on a vibration-free stage was used as the electrochemical cell. Both solutions were deaerated by N_2 bubbling for 15 min. The ITIES were then formed by pouring into the cell 0.7 mL of the aqueous solution (bottom layer) containing 1 M $NaClO_4$ + x M $Na_2C_2O_4$ (x = 0.06, 0.045, 0.03, 0.015) and then 0.7 mL of the BN solution (top layer) containing 2 mM $RuL_2L'^{2+}$ + 0.1 M $THAClO_4$.

Apparatus and Procedure. A home-built SECM instrument[37] was used for measurement of current, i_T, and of the ECL intensity, I_l, as a function of the tip−interface distance. The ECL intensity was measured via a photomultiplier tube (PMT, Hamamatsu R4220p) installed under the electrochemical cell and connected to an operational amplifier based current-to-voltage converter and voltage amplifier, as described previ-

ously.[24,38] In all SECM experiments, the tip electrode was positioned in the upper phase (BN) and a steady-state voltammogram of the $RuL_2L'^{2+}$ oxidation was recorded. The tip was then biased to the plateau current of the oxidation wave. When a steady current was attained, the tip was moved toward the ITIES while recording both i_T and I_l as a function of d, the tip−interface distance.

Results and Discussion

We now discuss the experimental SECM approach curves and their interpretation to obtain ET rate constants at the ITIES. As discussed previously, the approach curves depicting the electron transfer from a hydrophobic ruthenium complex such as $Ru(bpy)_2(C_{12}\text{-}bpy)^{3+}$ in BN to oxalate dianion in an aqueous phase show a minimum. Various phenomena that could interact with the interfacial ET could cause this deformation of the usual approach curve, including ion diffusion limitations or reactant transfer across the interface. The ion diffusion limitation does not apply in our case since, as discussed earlier,[16] oxalate ion that is oxidized at the liquid−liquid interface is in great excess compared to the ruthenium oxidant.

Ion-Transfer Limitations. Ion transfer of reactants across the BN−water interface could occur. Oxalate dianion is a small, highly hydrophilic molecule and should not transfer from water into BN. Hydrophobic ruthenium complexes such as $Ru(bpy)_2(C_{12}\text{-}bpy)^{2+}$ or the other RuL_3^{2+} species with L ≠ bpy or their oxidized counterparts should not cross the interface.

For less hydrophobic ruthenium complexes, such as $Ru(bpy)_3^{2+}$, transfer from organic to aqueous solution has been described and is feasible.[7,8] It is possible to minimize this transfer from organic to aqueous phase by increasing the Galvani potential difference. In the presence of another partitioning ion such as ClO_4^-, $Ru(bpy)_3^{2+}$ transfer from BN to aqueous solution is related to ("o" is the BN and "w" the water phase)

$$Ru(bpy)_3^{2+}{}_o + 2ClO_4^-{}_o \rightleftarrows Ru(bpy)_3^{2+}{}_w + 2ClO_4^-{}_w \quad (27)$$

The Galvani potential difference, $\Delta_w^\circ\varphi$, can be calculated by partitioning ion standard interfacial potential according to

$$\Delta_w^\circ\varphi = \Delta_w^\circ\varphi^0_{ClO_4^-} + \frac{RT}{F}\ln\frac{a_{ClO_4^-}{}^o}{a_{ClO_4^-}{}^w} = \Delta_w^\circ\varphi^0{}_{Ru^{2+}} + \frac{RT}{2F}\ln\frac{[Ru^{2+}]^w}{[Ru^{2+}]^o} \quad (28)$$

where $a_{ClO_4^-}{}^i$ corresponds to the activity of perchlorate anion in solvent i; in the concentration range of ruthenium complex, activities can be taken as equal to the concentration. Equation 27 shows that it is possible to minimize the Ru^{2+} transfer to aqueous solution by lowering the Galvani potential difference, i.e., by lowering the organic ClO_4^- concentration and increasing its concentration in the aqueous phase. Moreover, since a negative charge has to be transferred into the aqueous phase during the ET to maintain electroneutrality, a high perchlorate concentration in the BN phase is also advantageous to avoid kinetic limitations by ClO_4^- ion transfer.[11]

The difference in standard Galvani potential difference can be estimated from the partition equilibrium[1] of $Ru(bpy)_3(ClO_4)_2$ between BN and water. In such an experiment an aqueous $Ru(bpy)_3^{2+}$ solution (concentration $[Ru^{2+}]^t = 2$ mM) was mixed with an equal volume of BN. When equilibrium 27 was reached, the aqueous ruthenium concentration $[Ru^{2+}]^w$ was estimated by UV spectroscopy to be 0.43 mM. Equation 28 then becomes a simple function of $\Delta\Delta_w^\circ\varphi^0$, $[Ru^{2+}]^w$ and $[Ru^{2+}]^t = [Ru^{2+}]^w + [Ru^{2+}]^o$, the equilibrium aqueous concentration and the initial total ruthenium concentration, respectively:

$$\Delta\Delta_w^\circ\varphi^0 = \Delta_w^\circ\varphi^0_{Ru^{2+}} - \Delta_w^\circ\varphi^0_{ClO_4^-} = \frac{3}{2}\frac{RT}{F}\ln\left(\frac{[Ru^{2+}]^t}{[Ru^{2+}]^w} - 1\right) \quad (29)$$

leading to $\Delta\Delta_w^\circ\varphi^0 = 0.05$ V and with $\Delta_w^{BN}\varphi^0_{ClO_4^-} = 0.05$ V,[39] this leads to $\Delta_w^{BN}\varphi^0_{Ru(bpy)_3^{2+}} = 0.10$ V and $\Delta G^{0,w\rightarrow BN}_{Ru(bpy)_3^{2+}} = -0.2$ eV.

These constants ensure that under our SECM experimental conditions $Ru(bpy)_3^{2+}$ transfer into water is clearly negligible. Taking ClO_4^- activities equal to concentrations, one expects $[Ru(bpy)_3^{2+}]^w \approx [Ru(bpy)_3^{2+}]^o/5000 = 4 \times 10^{-7}$ M, and the interfacial potential will be fixed by the only potential-determining ion, ClO_4^-, common to the two phases.

Transfer of the ruthenium(III) complex was difficult to investigate in the same manner, because of its instability on the time scale of hours. Obviously, it should be easier to transfer into water than the ruthenium(II) counterpart, because it is more charged and thus more hydrophilic. However, the maximum quantity that could be transferred into the aqueous phase will be the solubility of the complex in a 1 M $NaClO_4$ aqueous solution, which should be low since $Ru(bpy)_3(ClO_4)_2$ salts can be readily obtained by addition of an excess of a perchlorate salt to a $Ru(bpy)_3^{2+}$ aqueous solution. Table 2 presents the solubilities in a 1 M $NaClO_4$ aqueous solution of $Fe(bpy)_3^{2+}$, $Fe(bpy)_3^{3+}$, $Ru(bpy)_3^{2+}$, $Ru(bpy)_3^{3+}$, $Ru(dmbp)_3^{2+}$, and $Ru(dmbp)_3^{3+}$ investigated systematically by UV spectroscopy.

TABLE 2: Concentration of ML_3 Complexes in Saturated 1 M $NaClO_4$ Aqueous Solutions Determined by UV Spectroscopy

complex ML_3	$[M(II)L_3]_{sat}$[a]	$[M(III)L_3]_{sat}$[a]	$[M(III)]_{sat}/[M(II)]_{sat}$
$Fe(bpy)_3$	3.5×10^{-6}	2.2×10^{-4}	63
$Ru(bpy)_3$	5.5×10^{-6}	1.5×10^{-4}	27
$Ru(dmbp)_3$	$<2 \times 10^{-7}$ [b]	2.3×10^{-6}	>12

[a] In M. [b] Detection limit.

The results confirmed the intuitive idea that the M(II) complexes are less soluble in the aqueous solution than their oxidized counterparts. This solubility depends more on the ligand than on the nature of the metal; iron- and ruthenium-[(tris(bipyridine)] complexes have similar solubilities. Replacing bipyridine by 4,4′-dimethylbipyridine greatly lowers the complex solubility. The $Ru(bpy)_3^{3+}$ transfer is then the most likely, but it still represents less than 1/13 of the initial $Ru(bpy)_3^{2+}$ concentration in the BN phase. Moreover, due to the ET reaction with the oxalate species that regenerate $Ru(bpy)_3^{2+}$ and then conservation of the ruthenium species, transfer of $Ru(bpy)_3^{3+}$ will also be dictated by $Ru(bpy)_3^{2+}$ transfer and solubility in the water phase and can be neglected as a first approximation (the effect of this ion transfer on the current passed through the interface is discussed later). This would be even truer for the other, more hydrophobic, ruthenium complexes. With high aqueous perchlorate ion concentrations we thus believe that transfer of ruthenium species from BN to the aqueous phase is quite unfavorable for all of the Ru complexes (except probably

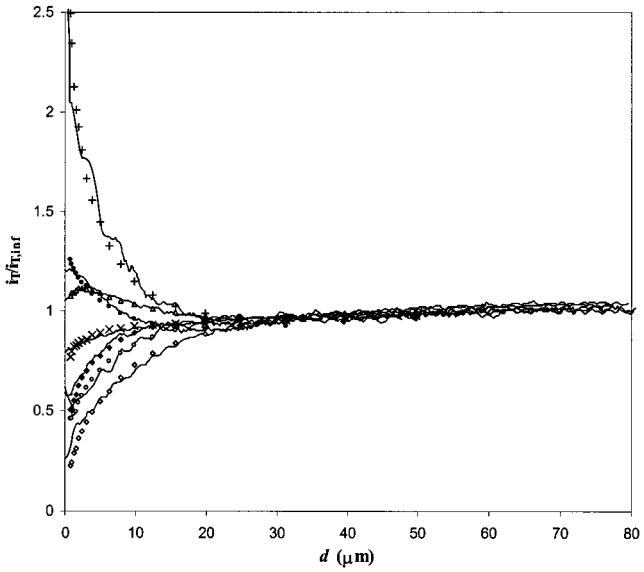

Figure 9. Experimental approach curves (lines) for the oxidation of 2 mM $RuL_2L'^{2+}$ in BN at an UME approaching a 0.06 M oxalate aqueous solution. The symbols represent the simulated approach curves for each complex using the model described herein. The ruthenium complexes were (+) **1**, (●) **2**, (△) **3**, (×) **4**, (◆) **5**, (○) **6**, and (◇) **7**.

$Ru(bpy)_3^{3+}$), and that the peculiar approach curves observed could not be attributed to kinetic limitations by ion transfer. The intervention of an irreversible homogeneous chemical transformation of the mediator is more likely.

Application of the Kinetic Model. The model presented previously to account for systems involving an irreversible homogeneous chemical reaction of the mediator coupled to slow heterogeneous electron transfer will be used to describe the oxalate oxidation across the BN−water interface.

As described earlier and as can be seen on the different experimental steady-state approach curves presented in Figure 9, a shallow minimum that is predicted by theory is observed. The experimental data are shown with the best fits from the model discussed above for different ruthenium mediators at a constant oxalate concentration in Figure 9 or for the same ruthenium complexes **1**, **2**, and **3** and different oxalate concentrations in Figure 10. The values of k_{het} and k_c extracted from the fits presented in Figure 9 are provided in Table 3. The fit is quite good with the same value of the chemical homogeneous decomposition rate constant, k_c, for a given mediator with different oxalate concentrations. The estimated heterogeneous electron-transfer rate constant is proportional to the oxalate concentration in the aqueous phase as can be seen in Figure 11. These observations tend to validate the hypothesis of kinetic limitations by the coupled decomposition reaction with rate constant k_c.

We tried to elucidate the nature of this homogeneous chemical reaction between the Ru(III) species and a component in the BN solution. It probably involves an electron-transfer step, since the value of the chemical reaction rate depended on the potential of the ruthenium complex used (see Table 3). The more oxidizing the ruthenium complex, the faster was the chemical reaction. Reaction with water has been described in the earlier work, but this does not seem too likely. It would be difficult to explain the approach curve with $Ru(bpy)_3^{3+}$ and the other less oxidizing ruthenium complexes that are known to have low reactivity with water. We believe the chemical reaction is due to the presence of a contaminant in the BN used. As a matter of fact, when a fresh lot of BN was used, the unusual behavior

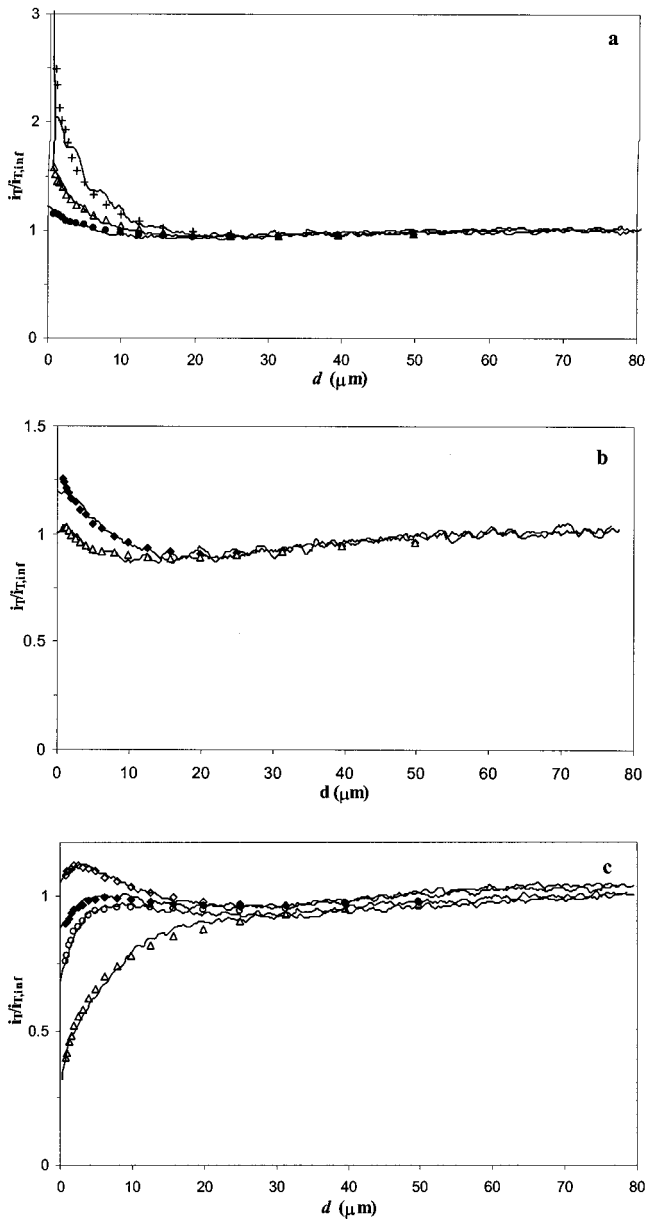

Figure 10. Experimental approach curves (lines) for the oxidation of 2 mM $RuL_2L'^{2+}$ in BN at an UME approaching an oxalate aqueous solution. The symbols represent the simulated approach curves for each complex and each oxalate concentration using the model described herein. The ruthenium complexes were (a) **1**, [oxalate] = (+) 0.06 M, (△) 0.03 M, (●) 0.015 M; (b) **2**, [oxalate] = (◆) 0.06 M, (△) 0.03 M; (c) **3**, [oxalate] = (◇) 0.06 M, (◆) 0.045 M, (○) 0.03 M, (△) 0.015 M.

attributed to chemical decomposition of the oxidizing reagent was absent. The new approach curves, obtained for **2** and **3**, resemble more closely the curves expected for a slow heterogeneous electron transfer without the interfering reaction. The heterogeneous rate constant extracted from these approach curves using the simpler model[11−14] are consistent with the values extracted in the contaminated BN lot when the competitive homogeneous chemical reaction was taken into account. Although we did not investigate further the nature of the interfering chemical step involved here, we believe it is due to prolonged contact of the BN with molecular sieve, which was not done with the new lot of BN.

ECE Mechanism at the Liquid−Liquid Interface. The oxalate dianion and the carbon dioxide radical anion are oxidized

TABLE 3: Oxidation of Oxalate by $RuL_2L'^{3+}$ at the BN−Water Interface

RuL_2L'	$\Delta E_{1/2}$[a]	k_{het}[b]	k_c[c]	β_t[d]
1	0.07_5	0.020[e]	1.1[e]	45 ± 10
2	0.02	0.0085[e]	1.3[e]	26 ± 5
2[f]	0.02	0.0082[e,f]		
3	$-\mathbf{0.01_5}$	0.0063[e]	0.65[e]	50 ± 10
3[f]	-0.01_5	0.0058[e,f]		
4	$-\mathbf{0.05_c}$	0.0030	0.5	18
5	$-\mathbf{0.07_5}$	0.0018	0.3	<11
6	$-\mathbf{0.09_5}$	0.0014	0.15	<13
7	$-\mathbf{0.17}$	0.0003_5	0	<19

[a] Difference in the substrate oxidation potentials (see text), in V. [b] Heterogeneous electron transfer rate constant in cm s^{-1} obtained for $[oxalate]^w = 0.06$ M. [c] Homogeneous irreversible chemical decay of Ru^{3+} in s^{-1}. [d] ECL light intensity proportionality factor, defined by (50), has the dimension of PMT output, in pA. [e] Value obtained from the average bimolecular rate constant extracted from oxalate concentration dependence. [f] Values obtained with the classical treatment in the fresh lot of BN.

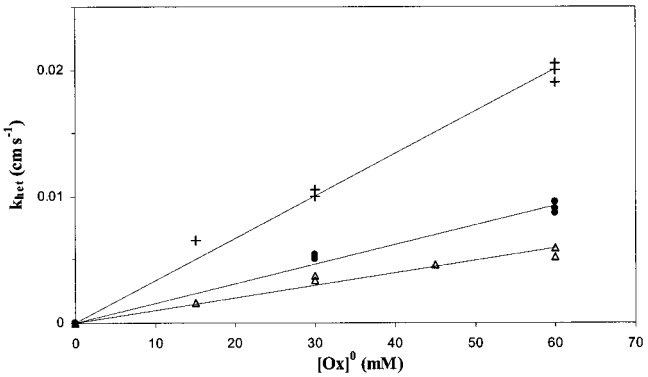

Figure 11. Variation of the measured heterogeneous ET rate constant, k_{het}, with the oxalate concentration for different Ru complexes: (+) **1**; (●) **2**; (△) **3**.

at the interface by the Ru(III) species in the BN producing the feedback current, denoted i_f, which is the sum of two contributions, i_1^{II} and i_2^{II}, corresponding respectively to the oxidation of $C_2O_4^{2-}$ and $CO_2^{\bullet -}$ and defined by

$$i_1^{II}/FA = D\frac{\partial[C_2O_4^{2-}]}{\partial z}|_{z=d} = k_{Ox}[Ru^{3+}]^o{}_d[C_2O_4^{2-}]^w{}_d \quad (30)$$

$$i_2^{II}/FA = D\frac{\partial[CO_2^{\bullet -}]}{\partial z}|_{z=d} = k_{CO}[Ru^{3+}]^o{}_d[CO_2^{\bullet -}]^w{}_d \quad (31)$$

where $[X]^i{}_d$ corresponds to the interfacial concentration of species X in phase i, k_{CO} represents the contribution of both reactions 3 and 3*, and A is the interfacial area.

Because of the high instability of $C_2O_4^{\bullet -}$,[22,40] oxalate oxidation is believed to proceed according to an ECE mechanism rather than a DISP one. Moreover, $CO_2^{\bullet -}$ is a strong reducing species whose oxidation according to (3) or (3*) is expected to be much faster than the first ET (1) and is probably diffusion limited. Therefore, under the steady-state conditions provided by the SECM technique, from a combination of the diffusion equations pertaining to $C_2O_4^{\bullet -}$ and $CO_2^{\bullet -}$ and the fact that their flux is zero at infinite distances, it is expected that $i_1^{II} = i_2^{II} = i_S$, where i_S is the current flowing through the interface. This was demonstrated previously for classical ECE systems controlled by a fast C and slow first E steps.[41]

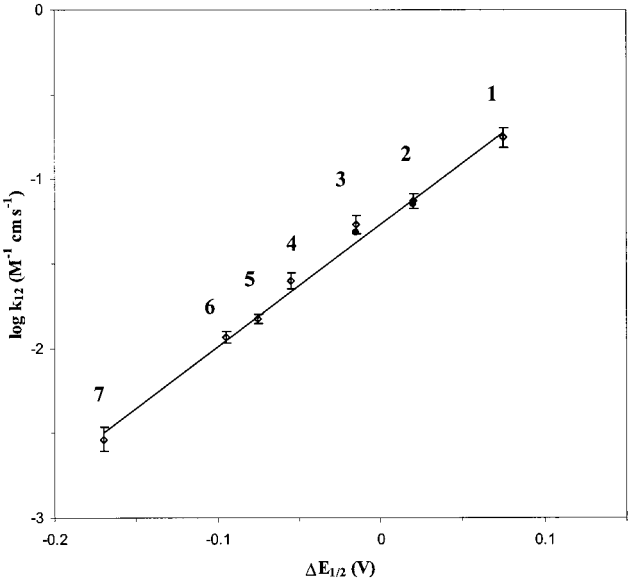

Figure 12. Variation of the bimolecular rate constant $k_{12} = k_{het}/2[Ox]^0$ with the driving force for oxalate oxidation by Ru complexes at the BN−water interface; from right to left **1**, **2**, **3**, **4**, **5**, **6**, **7** (◇) values extracted from the model described herein, (●) values extracted from classical treatment.

Hence, the current, i_S, that flows across the liquid−liquid interface is given by

$$i_S/FA = D\frac{\partial[Ru^{3+}]}{\partial z}|_{z=d} = 2i_1^{II} = 2k_{Ox}[Ru^{3+}]^o{}_d[C_2O_4^{2-}]^w{}_d \quad (32)$$

The process is then kinetically governed by the first slow ET step and two electrons are apparently transferred at a same rate k_{Ox}. The overall rate constant k_{het} that could be extracted from the approach curves is then twice the value of $k_{Ox}[C_2O_4^{2-}]^w{}_d$, the rate constant corresponding to step 1 in Scheme 1.

Influence of the Driving Force on the Interfacial Electron Transfer. From the approach curves obtained in BN for different mediators and the subsequent values of k_{het} gathered in Figure 9 and Table 3, one sees a clear trend: the more oxidizing the ruthenium complex, the higher the current crossing the interface.

One can then extend to all the ruthenium complexes the linear dependence of the heterogeneous ET rate constant with oxalate concentration observed in Figure 11 for the three more oxidizing couples and obtain the bimolecular ET rate constant $k_{12} = k_{het}/(2[Ox]^0)$, in M^{-1} cm s^{-1} corresponding to ET (1) in Scheme 1. The potential dependence of k_{12} is shown in Figure 13.The interfacial ET driving force, $\Delta G°$, generally includes the difference in standard potentials of the organic and aqueous redox couples and the Galvani potential difference:

$$\Delta G° = -(E°_{RuL_2L',o} - E°_{Ox,w}) - \Delta°_w\varphi = -\Delta E_{1/2} \quad (33)$$

It can be readily obtained by cyclic voltammetry determination of the formal potential of the involved redox mediators in their respective phases versus the same reference electrode placed in a constant phase, e.g., the aqueous phase.[14,16,42] Due to the irreversibility of the oxalate oxidation, a redox mediator, $Ru(CN)_6$,$^{4-}$ was placed in the aqueous phase and the formal potential difference between $Ru(CN)_6^{4-}$(w) and $RuL_2L'^{2+}$(o) oxidation was determined. The formal potential difference, $\Delta E_{1/2}$, between oxalate and $RuL_2L'^{2+}$ was then deduced from

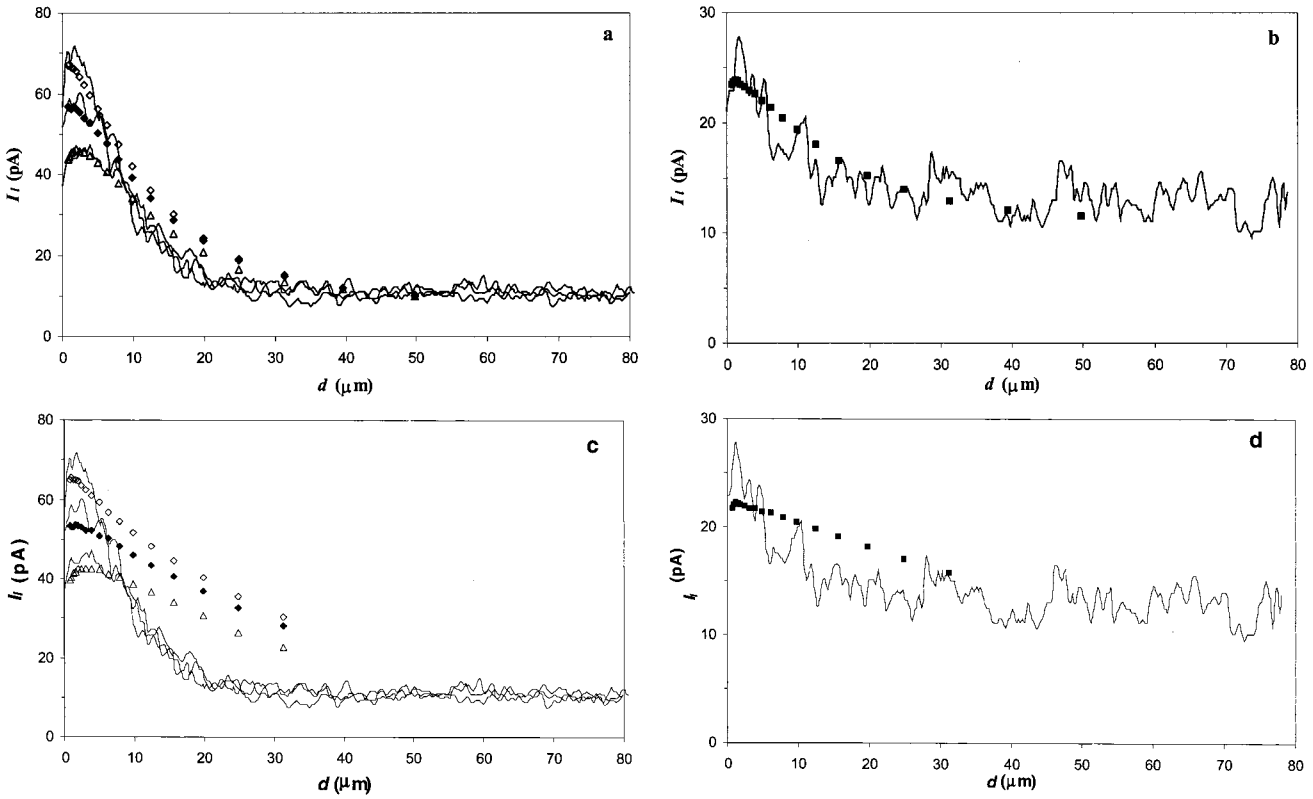

Figure 13. Experimental (solid line) and theoretical (symbols; according to $I_l = \beta_l(I_{T,theor} - I_{T,ins})/(1 - I_{T,ins}/I_{T,c}) + I_{dk}$; see text) variation of I_l, the ECL light intensity, with approach distance for oxalate oxidation by (a) **1**, (b) **2**, (c) **3**, or (d) **4** at the BN−water interface. (a) [**1**] = 2 mM, [oxalate] = 0.06 M; (b) [**2**] = 2 mM, [oxalate] = (◇) 0.06, (△) 0.03 M; (c) [**3**] = 2 mM, [oxalate] = (◇) 0.06, (◆) 0.045, (△) 0.03; (d) [**4**] = 2 mM, [oxalate] = 0.06 M.

the known values for the oxalate[22] and $Ru(CN)_6^{4-}$ standard potentials in water with respect to the same reference: NHE or $Ru(bpy)_3^{3+}/Ru(bpy)_3^{2+}$. The values of $\Delta G°$ for the different $RuL_2L'^{3+/2+}$ couples are given in Table 3.

Variations of the rate constant with driving force of electron transfer are expected to follow the Marcus activation−driving force relationship:[2]

$$\Delta G^{\ddagger} = \Delta G^{\ddagger\circ}(1 + \Delta G°/4\Delta G^{\ddagger\circ})^2 \qquad (34)$$

where $\Delta G^{\ddagger}$ and $\Delta G^{\ddagger\circ}$ are the free activation energy and the intrinsic activation energy (free activation energy at zero driving force), respectively, with

$$\Delta G^{\ddagger} = -RT/F \ln(k_{12}/Z) \qquad (35)$$

where Z is a preexponential factor for the electron transfer. For low driving forces (34) can be approximated by a Butler−Volmer-type linear law (36) that is usually adopted for low-overvoltage ET reactions at a liquid−liquid interface,[2,13,14,19,20] but also for typical endergonic homogeneous redox catalysis of ECE reaction:

$$\Delta G^{\ddagger} = \alpha\Delta G° + \Delta G^{\ddagger\circ} \qquad (36)$$

where α is the apparent electron-transfer coefficient.

The dependence of the rate constant on the Galvani potential drop has been studied experimentally and has been attributed on experimental[9,17,45,46] or theoretical[3,6] grounds to both diffuse-layer effects that reflect the work necessary to bring the charged reactants to the interface[3] and to a Butler−Volmer trend.[13] In our case, the Galvani potential drop remained constant and only the $E°$ of the mediator in the BN phase was changed, so that (34) should be valid, as for homogeneous ET.[2,17] Such dependence of the ET rate constant on $\Delta E°$ has been already observed experimentally[14,16] and has been questioned by a recent investigation of ET at an ITIES by a thin-layer technique.[10] However, a theoretical model of the latter technique suggested that the apparent independence of the ET with $\Delta E°$ could rather reflect diffusional limitations in the lower phase.[47]

In the case of oxalate oxidation at ITIES, log k_{12} varied linearly with the driving force of the electron transfer. From the linear plot in Figure 12, an apparent coefficient transfer $\alpha = \partial\Delta G^{\ddagger}/\partial\Delta G° = RT/F\ \partial \ln k_{12}/\partial\Delta G° = 0.43$ is deduced. This value is comparable to the one obtained for heterogeneous oxalate oxidation at a carbon electrode in an aprotic solvent[25] and seems low compared to the one extracted from the homogeneous oxidation in aqueous solution of oxalate by ruthenium complexes ($\alpha_{hom} = 0.6$).[22] Such a difference between homogeneous and heterogeneous transfer coefficients is often seen[44] and has been interpreted, according to the quadratic aspect of Marcus law, as the more exothermic driving force involved in the interfacial ET (for $Ru(bpy)_3^{2+}$ at the ITIES $\Delta G°_{12} = 0.015$ eV) than in the homogeneous case (for $Ru(bpy)_3^{2+}$ $\Delta G°_{hom} = 0.2$ eV).

From the linear Tafel plot of oxalate oxidation at the BN−water interface, one may extrapolate to zero driving force and obtain the bimolecular rate constant for oxalate oxidation, $k_{12}^{II,0} = 0.054\ M^{-1}\ cm\ s^{-1}$. This value is close to those reported for ET between $ZnPor^+$ and $Ru(CN)_6^{4-}$ at the benzene−water interface ($k_{12}° = 0.084\ M^{-1}\ cm\ s^{-1}$) or between $FcCOO^-$ and Fc at the water−nitrobenzene interface ($k_{12}° = 0.06\ M^{-1}$ cm

s^{-1}).[12,14] Our slightly lower value could represent the higher reorganization energy needed for the oxalate oxidation.[22,25]

We attempted to compare this value to Marcus' theoretical predictions.[2] Two different physical descriptions of the liquid−liquid interface have been proposed according to whether the ET occurs at a sharp, planar boundary layer of thickness $\Delta R \sim 1$ Å or in a deeper interfacial region of thickness L, typically several layers of mixed solvent. The theoretical bimolecular rate constant k_{12}^{ll} is given for the two possibilities by the following expressions:

$$k_{12}^{ll} = 2\pi(a_1 + a_2)(\Delta R)^3 \kappa\nu_n \exp(-F\Delta G^{\ddagger}/RT) \quad (37)$$

and

$$k_{12}^{ll} = 4\pi(a_1 + a_2)^2 \Delta R L \kappa\nu_n \exp(-F\Delta G^{\ddagger}/RT) \quad (38)$$

where $a_1$and a_2 represent the reactants' radii, $\kappa\nu_n$ is the product of the adiabaticity factor by a frequency of nuclear motion (typically $\kappa\nu_n = 10^{12}$ cm s^{-1}). We used the formalism adopted by Marcus in order to compare the ET rates constants at zero driving force of the homogeneous electron transfer rate constant ($k_{12,w} = 7 \times 10^5$ M^{-1} s^{-1} extrapolated from previous work), to the theoretical values predicted by the Marcus formalism for the liquid−liquid interface, $k_{12}^{ll,0}$. The procedure is based on the additivity of reorganization energies, λ:

$$\lambda_{12}^{ll} = (1/2)(\lambda_{11,o} + \lambda_{22,w}) \quad (39)$$

where λ_{12}^{ll} and $\lambda_{ii,j}$ represent the reorganization energies for the liquid−liquid ET or for the self-exchange reaction between the oxidized forms of reactant i in liquid j, respectively.

From the expression of the rate constant of homogeneous ET[48]

$$k_{12} = 4\pi(a_1 + a_2)^2 \Delta R \kappa\nu_n \exp(-F\Delta G^{\ddagger}/RT) \quad (40)$$

where k_{12} refers to the same reaction when the reactants are in the same homogeneous phase. The self-exchange rate constants for reactant i in each solvent j, $k_{ii,j}$ follows directly from (40). From the formalism adopted in the homogeneous case, one can derive relations between the various rate constants at zero driving force at the liquid−liquid interface:

$$k_{12}^{ll,0} = (\Delta R)^2(a_1 + a_2)(k_{11,o}k_{22,w})^{1/2}/(8a_1a_2) \quad (41)$$

in the case of a sharp boundary layer, or

$$k_{12}^{ll,0} = (a_1 + a_2)^2 L(k_{11,o}k_{22,w})^{1/2}/(4a_1a_2) \quad (42)$$

in the case of a thicker interfacial region.

For the same homogeneous reaction but in the aqueous phase, the zero-energy cross-exchange rate constant is then given by

$$k_{12,w}^{0} = (a_1 + a_2)^2(k_{11,w}k_{22,w})^{1/2}/(4a_1a_2) \quad (43)$$

To relate $k_{12}^{ll,0}$ to the homogeneous $k_{12,w}^{0}$ value obtained in water, we need an estimate of the change in the self-exchange rate constant for any $RuL_3^{3+/2+}$ when passing from water to BN. A recent study of $Ru(phen)_3^{2+}$ [49] or $Co(bpy)_3^{2+}$ [50] electrochemical oxidation showed that, for such metal complexes, the nature of the solvent only affected the preexponential factor of the heterogeneous ET rate constant through the Pekar factor ($1/n_{op}^2 - 1/\epsilon_s$) and the longitudinal solvent relaxation time, τ_L, proving that the electrode reaction was "perfectly" adiabatic. Thus, the homogeneous ET of these compounds and other $RuL_2L^{3+/2+}$ analogues is expected to be adiabatic, too. The change in electron self-exchange rate constant should not depend on the nature of the complex but rather follow the trends observed for other adiabatic couples such as $CpCo^{+/0}$,[51] for whose self-exchange rate constant in BN is 1/10 of the water value. We can then assign the same ratio to the corresponding ruthenium rate constants, $k_{11,o} \sim k_{11,w}/10$, and can relate $k_{12}^{ll,0}$ to $k_{12,w}^{0}$ for the sharp boundary model:

$$k_{12}^{ll,0} \sim 0.3(\Delta R)^2/(2a_1 + 2a_2)k_{12,w}^{0} \quad (44)$$

or for the model involving ET in a thicker solvent layer:

$$k_{12}^{ll,0} \sim 0.3Lk_{12,w}^{0} \quad (45)$$

Using $a_1 = 6.8$ Å[52] and $a_2 = 2$ Å,[53] we estimate $k_{12}^{ll,0} \sim 10^{-4}$ M^{-1} cm s^{-1} from (44). This seems low compared to our experimental value (0.054 M^{-1} cm s^{-1}) and seems to disfavor the sharp boundary layer model. It rather might suggest that the ET occurs in an interfacial boundary region of mixed solvent whose dimension can be estimated from (45) to $L \sim 2$ nm. This value could reflect the higher mutual solubility of water with BN than with more usual DCE or nitrobenzene used in ITIES studies. This finding is also consistent with the frequently adopted three-layer model of the ITIES that predicts the absence of a log k_{12}^{ll} dependence with the Galvani potential drop.[4−6] However, other studies have shown variation of heterogeneous reaction rate with this Galvani potential drop.[14−16,54]

In the special case of **3** (and likely **4** to a lesser extent), some Ru^{3+} transfer from the BN to the water phase could explain the higher bimolecular ET rate constant. This would agree with the occurrence of the ET in a thicker reaction layer as was also observed for Fc partitioning during its oxidation by $FcCOO^-$ at the water−nitrobenzene interface.[12] The ET would then occur either heterogeneously at the liquid−liquid interface or homogeneously in an aqueous reaction layer with respective rate constants k_h and k_{hom}. Due to the high oxalate concentration, both reactions can be considered as pseudofirst order. One could estimate, from previous work, the homogeneous aqueous reaction layer to be about $(D/(2k_{hom}[Ox]^0))^{1/2} = a/\lambda_{hom} \sim 0.7$ μm for $[Ox]^0 = 0.06$ M. The current flowing through the ITIES due to $Ru(bpy)_3^{3+}$ ion transfer from the organic to the aqueous phase is given by[32h]

$$i_{IT}/FA = D\frac{\partial[Ru^{3+}]^w}{\partial z}|_{z=d} = k_w([Ru^{3+}]^w_d - K_p[Ru^{3+}]^o_d)$$

where k_w is the rate constant for Ru^{3+} ion transfer from water to BN and K_p its partition equilibrium constant. The SECM configuration provides that $[Ru^{3+}]$ values are constants on both sides of the interface; then one can find by solution of the steady-state diffusion equation for $[Ru^{3+}]^w$ that

$$i_{IT} = FAD\frac{(1 + \lambda_{hom})\lambda_w}{1 + \lambda_{hom} + \lambda_w}K_p[Ru^{3+}]^o_d \sim \frac{\lambda_{hom}\lambda_w}{(\lambda_{hom} + \lambda_w)\lambda_{het}}K_p i_{ET}$$

with $\lambda_w = k_w a/D$, $\lambda_{het} = k_{het}a/D$, and i_{ET}, the current flowing through the interface due to heterogeneous ET, is given by i_S in (32).

From the ion solubility study and due to the Ru species conservation and the homogeneous conversion of the aqueous Ru^{3+} into Ru^{2+}, the highest value for $[Ru^{3+}]^w$ is given by the solubility of Ru^{2+} ion in the 1 M $NaClO_4$ aqueous phase; therefore K_p is at most 1/360. From the value of k_{het} extracted from this work, one could estimate that IT would represent less

than $\lambda_{hom}K_p/\lambda_{het} \sim 4-6\%$ (in the oxalate concentration range) of the current flowing through the ITIES.[55] For the other Ru complexes, Ru ion transfers can be neglected

ECL Generation at the Liquid−Liquid Interface. Once the first electron transfer has occurred, the $CO_2^{\bullet -}$ radical anion produced by fragmentation of the oxalate radical anion $C_2O_4^{\bullet -}$ can be further oxidized by a second electron transfer to $RuL_2L'^{3+}$, steps 3 and 3* in Scheme 1. These steps are certainly faster than the rate-limiting step, the formation of $C_2O_4^{\bullet -}$ by (1), and lead to a competitive formation of the Ru^{2+} species in its ground or excited state. The formation of the excited state leads to light emission. Therefore, as soon as the tip approaches the BN−water interface there is enough feedback to generate an emitting species by subsequent electron transfer across the interface. This effect is characterized by observation of photon emission.[24] Figure 13 presents the emission intensity, I_l, as a function of the tip−interface distance. This emission is weak and close to the accessible range of our light measurement device, but still quantifiable for the four most strongly oxidizing ruthenium complexes. The approach to that developed in the homogeneous oxalate oxidation[22] has been transposed here to rationalize the light emission. The light intensity, I_l, is proportional to the rate of radiative decay of $Ru^{2+}*$

$$I_l \propto k_r[Ru^{2+}*] \tag{46}$$

where k_r is the radiative decay rate constant of the Ru^{2+} excited state. It should also be proportional to the flux corresponding to $Ru^{2+}*$ generation; therefore

$$I_l \propto k_r/(k_r + k_{nr})k_{3*}[Ru^{3+}]^o_0[CO_2^{\bullet -}]^w_0 \tag{47}$$

where k_{nr} is the rate constant for nonradiative decay of $Ru^{2+}*$.

Combining (30) and (32) that express this flux as a function of the current, i_S, flowing through the interface, one obtains

$$I_l \propto \frac{k_r}{k_r + k_{nr}} \frac{k_{3*}}{k_3 + k_{3*}} i_S/2 \tag{48}$$

an expression which is similar to that obtained for the homogeneous oxidation.[22] As a first approximation, and for a distance $0 < L \leq 2$, this normalized interfacial current, I_S, is given by[11,14,20,56]

$$I_S = (I_T - I_{Tins})/(1 - I_{Tins}/I_{Tc}) \tag{49}$$

where I designates the normalized current, $I = i/i_{inf}$, and I_{Tc} corresponds to the tip current with a conductive substrate.

Since we attempted to simulate the variation of the tip current with the tip−interface distance, we also attempted to simulate the variation of the light emission with the distance. If we assume the presence of a dark signal, I_{dk}, due to detector background and stray light, we expect that I_l follows

$$I_l = \beta_l I_S + I_{dk} \tag{50}$$

In Figure 13, the symbols show the predicted variations of the light emission according to (50), when the substrate current is estimated from the simulated tip current according to the theoretical model developed here. The agreement between experimental and simulated variables is reasonable when the tip is close to the interface for the different cases. The agreement is worse for **3** at distances greater than 10 μm. The corresponding values of β_l extracted are presented in Table 3. To assess the validity of the model, we tested (50) for different oxalate concentrations in the cases of **2** and **3**. In each case the proportionality coefficient β_l was constant in the same series of experiment, as can be observed for **1**, **2**, and **3** in Figure 13, which lends further confidence in this analysis.

Because of the low light level (close to the noise level of the dark current for $Ru(bpy)_2dmbp^{2+}$ and at the dark current level for the other less positive compounds), it was difficult to investigate further the light emission and its driving force dependence. In any case for compounds less positive than **4**, we could estimate a maximum β_l factor by considering that the absence of a signal would indicate a signal that was, at most, equal to the noise level of the dark current. These maximum β_l values reported in Table 2 for **5**, **6**, and **7** are of the order of magnitude of values obtained for the four other complexes.

These results can be compared to the homogeneous oxalate oxidation in aqueous solution. In the latter case, the normalized β_l value (0.09) is approximately 10 times higher than that obtained at the liquid−liquid interface. It is difficult to give any mechanistic interpretation of this result, however, because of the possible presence of oxygen in the aqueous and BN phases.

Conclusion

The SECM approach curves describing the oxidation of oxalate by $RuL_2L'^{3+}$ complexes at the BN−water interface were investigated. The approach curves must be interpreted in terms of a homogeneous chemical degradation of $RuL_2L'^{3+}$ in addition to the interfacial ET. We thus developed a treatment for SECM feedback for the case of a finite heterogeneous ET in competition with homogeneous (first-order) decay of the mediator, which has been used to describe oxalate oxidation by Ru complexes at the BN−water interface. The homogeneous chemical degradation of the Ru(III) species is related to an impurity present in benzonitrile. The interfacial ET rate constants obtained for these systems show a linear activation−driving force relationship. Application of Marcus theory fits a model involving a 2 nm thick mixed solvent layer better than that for a sharp boundary.

The formation of $CO_2^{\bullet -}$ is demonstrated by detection of light emission during the reaction. The ECL intensity could be related to the current crossing the liquid−liquid interface, but is still too low to allow any detailed interpretation according to Marcus theory.

Acknowledgment. The authors thank Drs. Fu-Ren Frank Fan and Shigeru Amemiya for helpful discussions. The financial support of this research by grants from the National Science Foundation (CHE-9870762) and Robert A. Welch Foundation is gratefully acknowledged.

References and Notes

(1) For a review, see: (a) Girault, H. H.; Schiffrin, D. J. In *Electroanalytical Chemistry*; Bard, A. J., Ed.; Marcel Dekker: New York, 1989; Vol. 15, p 1. (b) Girault, H. H. In *Modern Aspects of Electrochemistry*; Bockris, J. O'M., Conway, B. E., White, R. E., Eds.; Plenum Press: New York, 1993; Vol. 25, p 1.

(2) (a) Marcus, R. A. *J. Phys. Chem.* **1990**, *94*, 1050. (b) Marcus, R. A. *J. Phys. Chem.* **1990**, *94*, 4152; Addendum. *J. Phys. Chem.* **1990**, *94*, 7742. (c) Marcus, R. A. *J. Phys. Chem.* **1991**, *95*, 2010; Addendum. *J. Phys. Chem.* **1995**, *99*, 5742.

(3) (a) Kharkats, Yu. I.; Volkov, A. G. *J. Electroanal. Chem.* **1985**, *184*, 435. (b) Kharkats, Yu. I.; Ulstrup, J. *J. Electroanal. Chem.* **1991**, *308*, 71.

(4) Girault, H. H.; Schiffrin, D. J. *J. Electroanal. Chem.* **1988**, *244*, 15.

(5) Katano, H.; Maeda, K.; Senda, M. *J. Electroanal. Chem.* **1995**, *396*, 391.

(6) Schmickler, W. *J. Electroanal. Chem.* **1997**, *428*, 123.
(7) Marecek, V.; De Armond, A. H.; De Armond, M. K. *J. Am. Chem. Soc.* **1989**, *111*, 2561.
(8) (a) Thomson, F. L.; Yellowlees, L. J.; Girault, H. H. *J. Chem. Soc., Chem. Commun.* **1988**, 1547. (b) Brown, A. R.; Yellowlees, L. J.; Girault, H. H. *J. Chem. Soc., Faraday Trans.* **1993**, *89*, 207. (c) Ding, Z.; Wellington, R. G.; Brevet, P. F.; Girault, H. H. *J. Phys. Chem.* **1996**, *100*, 10658.
(9) (a) Ding, Z. Fermin, D. J.; Brevet, P.-F.; Girault, H. H. *J. Electroanal. Chem.* **1998**, *458*, 139. (b) Fermin, D. J.; Ding, Z.; Duong. H. D.; Brevet, P.-F.; Girault, H. H. *J. Phys. Chem. B* **1998**, *102*, 10334.
(10) (a) Shi, C.; Anson, F. C. *Anal. Chem.* **1998**, *70*, 3114. (b) Shi, C.; Anson, F. C. *J. Phys. Chem. B* **1998**, *102*, 9850. (c) Shi, C.; Anson, F. C. *J. Phys. Chem. B* **1999**, *103*, 6283.
(11) (a) Bard, A. J.; Fan, F.-R. F.; Mirkin, M. V. In *Electroanalytical Chemistry*; Bard, A. J., Ed.: Marcel Dekker: New York, 1994; Vol. 18, p 243. (b) *Scanning Electrochemical Microscopy*; Bard, A. J., Mirkin, M. V., Eds.; Marcel Dekker: New York, 2001.
(12) Wei, C.; Bard, A. J.; Mirkin, M. V. *J. Phys. Chem.* **1995**, *99*, 16033.
(13) Tsionsky, M.; Bard, A. J.; Mirkin, M. V. *J. Phys. Chem.* **1996**, *100*, 17881.
(14) Tsionsky, M.; Bard, A. J.; Mirkin, M. V. *J. Am. Chem. Soc.* **1997**, *119*, 10785.
(15) Delville, M. H.; Tsionsky, M.; Bard, A. J. *Langmuir* **1998**, *14*, 2774.
(16) Barker, A. L.; Unwin, P. R.; Amemiya, S.; Zhou, J.; Bard, A. J. *J. Phys. Chem. B* **1999**, *103*, 7260.
(17) Amemiya, S.; Ding, Z.; Zhou, J.; Bard, A. J. *J. Electroanal. Chem.* **2000**, *483*, 7.
(18) Liu, B.; Mirkin, M. V. *J. Am. Chem. Soc.* **1999**, *121*, 8352.
(19) Zhang, J.; Unwin, P. R. *J. Phys. Chem. B* **2000**, *104*, 2341.
(20) Shao, Y.; Mirkin, M. V.; Rusling, J. F. *J. Phys. Chem. B* **1997**, *101*, 3202.
(21) (a) Rubinstein, I.; Bard, A. J. *J. Am. Soc. Chem.* **1981**, *103*, 512. (b) Rubinstein, I.; Martin, C. R.; Bard, A. J. *Anal. Chem.* **1983**, *55*, 1580.
(22) Kanoufi, F.; Bard, A. J. *J. Phys. Chem. B* **1999**, *103*, 10469.
(23) Rubinstein, I.; Bard, A. J. *J. Am. Chem. Soc.* **1981**, *103*, 5007.
(24) Zu, Y.; Fan, F.-R. F.; Bard, A. J. *J. Phys. Chem. B* **1999**, *103*, 6272.
(25) Isse, A. A.; Gennaro, A.; Maran, F. *Acta Chem. Scand.* **1999**, *53*, 1013.
(26) (a) D'Angelantonio, M.; Mulazzani, Q. G.; Venturi, M.; Ciano, M.; Hoffman, M. Z. *J. Phys. Chem.* **1991**, *95*, 5121. (b) Venturi, M.; Mulazzani, Q. G.; D'Angelantonio, M.; Ciano, M.; Hoffman, M. Z. *Radiat. Phys. Chem.* **1991**, *37*, 449.
(27) Schwarz, H. A.; Creutz, C.; Sutin, N. *Inorg. Chim.* **1985**, *24*, 433.
(28) Unwin, P. R.; Bard, A. J. *J. Phys. Chem.* **1991**, *95*, 7814.
(29) Demaille, C.; Unwin, P. R.; Bard, A. J. *J. Phys. Chem.* **1996**, *100*, 14137.
(30) Peaceman, D. W.; Rachford, H. H. *J. Soc. Ind. Appl. Math.* **1955**, *3*, 28.
(31) (a) Bard, A. J.; Mirkin, M. V.; Unwin, P. R.; Wipf, D. O. *J. Phys. Chem.* **1992**, *96*, 1861. (b) Pierce, D. T.; Unwin, P. R.; Bard, A. J. *Anal. Chem.* **1992**, *64*, 1795. (c) Unwin, P. R.; Bard, A. J. *J. Phys. Chem.* **1992**, *96*, 5035.
(32) (a) Macpherson, J. V.; Unwin, P. R. *J. Phys. Chem.* **1994**, *98*, 1704. (b) Macpherson, J. V.; Unwin, P. R. *J. Phys. Chem.* **1994**, *98*, 3109. (c) Macpherson, J. V.; Unwin, P. R. *J. Phys. Chem.* **1995**, *99*, 3338. (d) Macpherson, J. V.; Unwin, P. R. *J. Phys. Chem.* **1995**, *99*, 14824. (e) Macpherson, J. V.; Unwin, P. R. *J. Phys. Chem.* **1996**, *100*, 19475. (f) Slevin, C. J.; Macpherson, J. V.; Unwin, P. R. *J. Phys. Chem. B* **1997**, *101*, 10851. (g) Martin, R. D.; Unwin, P. R. *J. Electroanal. Chem.* **1997**, *439*, 123. (h) Barker, A. L.; Macpherson, J. V.; Slevin, C. J.; Unwin, P. R. *J. Phys. Chem. B* **1998**, *102*, 1586.
(33) Ames, W. F. *Numerical Methods of Partial Differential Equations*; Wiley: New York, 1977.
(34) Mirkin, M. V.; Fan, F.-R. F.; Bard, A. J. *J. Electroanal. Chem.* **1992**, *328*, 47.
(35) (a) Sprintschnik, G.; Sprintschnik, H. W.; Kirsch, P. P.; Whitten, D. G. *J. Am. Chem. Soc.* **1977**, *99*, 4947. (b) Braddock, J. N.; Meyer, T. J. *J. Am. Chem. Soc.* **1973**, *95*, 3158. (c) Lin, C.-T.; Bottcher, W.; Chou, M.; Creutz, C.; Sutin, N. *J. Am. Chem. Soc.* **1976**, *98*, 6536.
(36) (a) Bard, A. J.; Fan, F.-R. F.; Kwak, J.; Lev, O. *Anal. Chem.* **1989**, *61*, 1794. (b) Fan, F.-R. F In *Scanning Electrochemical Microscopy*; Bard, A. J., Mirkin, M. V., Eds.; Marcel Dekker: New York, 2001; Chapter 3.
(37) Wipf, D. O.; Bard, A. J. *J. Electrochem. Soc.* **1991**, *138*, 489.
(38) Fan, F.-R. F.; Cliffel, D.; Bard, A. J. *Anal. Chem.* **1998**, *70*, 2941.
(39) Alemu, H.; Solomon, T. *J. Electroanal. Chem.* **1989**, *261*, 297.
(40) (a) Prasad, D. R.; Hoffman, M. Z.; Mulazzani, Q. G.; Rodgers, M. A. J. *J. Am. Chem. Soc.* **1986**, *108*, 5153. (b) Mulazzani, Q. G.; D'Angelantino, M.; Venturi, M.; Hoffman, M. Z.; Rodgers, M. A. J. *J. Phys. Chem.* **1986**, *90*, 5347. (c) Pina, F.; Mulazzani, Q. G.; Venturi, M.; Ciano, M.; Balzani, V. *Inorg. Chem.* **1985**, *24*, 848.
(41) (a) Nadjo, L.; Savéant, J.-M. *J. Electroanal. Chem.* **1973**, *48*, 113. (b) Amatore, C.; Savéant, J.-M. *J. Electroanal. Chem.* **1977**, *85*, 27.
(42) Shafer, H. O.; Derbavk, T. L.; Koval, C. A. *J. Phys. Chem. B* **2000**, *104*, 1025.
(43) (a) Glebewicz, G.; Schiffrin, D. J. *J. Electroanal. Chem.* **1988**, *244*, 27. (b) Cunnane, V. J.; Schiffrin, D. J.; Beltran, C.; Geblewicz, G.; Solomon, T. *J. Electroanal. Chem.* **1988**, *247*, 203. (c) Cheng, Y.; Schiffrin, D. J. *J. Electroanal. Chem.* **1991**, *314*, 153.
(44) See, for example: Savéant, J.-M. In *Advances in Electron-Transfer Chemistry*; Mariano, P. S., Ed.; JAI Press: New York, 1994; p 53.
(45) Cheng, Y.; Schiffrin, D. J. *J. Chem. Soc., Faraday Trans.* **1993**, *89*, 199.
(46) Samec, Z.; Marecek, V.; Weber, J.; Homolka, D. *J. Electroanal. Chem.* **1981**, *126*, 105.
(47) Barker, A. L.; Unwin, P. R. *J. Phys. Chem. B* **2000**, *104*, 2330.
(48) Marcus, R. A. *J. Chem. Phys.* **1965**, *43*, 679.
(49) Winkler, K.; McNight, N.; Fawcett, W. R. *J. Phys. Chem. B* **2000**, *104*, 3575.
(50) Pyati, R.; Murray, R. W. *J. Am. Chem. Soc.* **1996**, *118*, 1743.
(51) Weaver, M. J. *Chem. Rev.* **1992**, *92*, 463.
(52) Sutin, N.; Creutz, C. *Adv. Chem. Ser.* **1978**, *168*, 1.
(53) Pederson, B. F.; Pederson, B. *Acta Chem. Scand.* **1964**, *18*, 1454.
(54) Ding, Z.; Quinn, B. M.; Bard, A. J., submitted.
(55) (a) The ion transfer rate constant could be approximated as 10^{-1} cm s^{-1}, a typical value for most ion transfer across water−DCE or water−nitrobenzene interfaces,[1,55b] leading to $\lambda_w \sim 2 \times 10^4$ of the same magnitude as λ_{hom}, and to $I_{IT}/I_{ET} \sim 0.02-5$. (b) Samec, Z. *Electrochim. Acta* **1998**, *44*, 125.
(56) (a) Mirkin, M. V.; Bulhoes, L. O. S.; Bard, A. J. *J. Am. Chem. Soc.* **1993**, *115*, 201. (b) Mirkin, M. V.; Arca, M.; Bard, A. J. *J. Phys. Chem.* **1993**, *97*, 10790. (c) Treichel, D. A.; Mirkin, M. V.; Bard, A. J. *J. Phys. Chem.* **1994**, *98*, 5751.